Calculating Core-Level Excitations and X-Ray Absorption Spectra of Medium-Sized Closed-Shell Molecules with the Algebraic-Diagrammatic Construction Scheme for the Polarization Propagator

Jan Wenzel,* Michael Wormit, and Andreas Dreuw*

Core-level excitations are generated by absorption of high-energy radiation such as X-rays. To describe these energetically high-lying excited states theoretically, we have implemented a variant of the algebraic-diagrammatic construction scheme of second-order ADC(2) by applying the core-valence separation (CVS) approximation to the ADC(2) working equations. Besides excitation energies, the CVS-ADC(2) method also provides access to properties of core-excited states, thereby allowing for the calculation of X-ray absorption spectra. To demonstrate the potential of our implementation of CVS-ADC(2), we have chosen medium-sized molecules as examples that have either biological importance or find application in organic electronics. The calculated results of CVS-ADC(2) are compared with standard TD-DFT/B3LYP values and experimental data. In particular, the extended variant, CVS-ADC(2)-x, provides the most accurate results, and the agreement between the calculated values and experiment is remarkable. © 2014 Wiley Periodicals, Inc.

DOI: 10.1002/jcc.23703

Introduction

Over the last years, X-ray absorption spectroscopy (XAS) has been improved due to modern synchrotron soft beam sources.[1,2] Techniques like near-edge soft X-ray absorption fine structure (NEXAFS) spectroscopy or X-ray absorption near-edge structure spectroscopy are widely used in many fields such as organic electronics and medical biological research.[2–5] For example, the peak structure of the core absorption spectra of the deoxyribonucleic acid (DNA) bases cytosine and uracil was analyzed to determine the population of specific tautomers.[4] Furthermore, the band structure of polythiophenes as electrically conducting polymers has been probed to understand their conduction mechanisms.[6] As the initially excited states are element specific and strongly localized, especially in K-edge spectroscopy due to the contracted 1s orbital, they serve as chemical fingerprint and afford information about the chemical structure of a compound as well as the orientation between adsorbed molecules.[7–9] Especially, NEXAFS techniques are used to probe excitations from the core region into unoccupied orbital levels of intramolecular bonds or extramolecular neighbors like surface atoms.[8] Furthermore, core-level excitations play an important role in processes known as intermolecular Coulombic decay (ICD), which has been first formulated in 1997.[10] An electronically excited molecule placed in a molecular environment efficiently decays by transfer of its excess energy to a neighboring molecule, which subsequently emits a low-energy electron.[11–13] Recent works confirm that such ICD processes can originate from core-excited states through a cascade mechanism, which lead to possible applications in radiation biology and cancer radiotherapy.[14,15] The ionic state undergoing ICD can be formed after de-excitation of a core-excited state via a local spectator Auger decay. In case of N_2, ICD competes for example with energy relaxation through dissociation without releasing an electron.[15]

Quantum chemical calculations aim at analyzing and interpreting the experimental spectra. As molecules present in organic electronics or in a biological context are usually large, time-dependent density-functional theory (TD-DFT)[16–18] is the method of choice to describe such systems in reasonable computational time. The self-interaction error (SIE) of TD-DFT as well as the empirical character of exchange-correlation (xc) functionals require an xc-functional evaluation for every investigated system.[19] Furthermore, the SIE in conjunction with the small gap between occupied and unoccupied orbitals derived from the DFT Kohn–Sham formalism lead to a generally strong underestimation of core excitation energies in TD-DFT making absolute shifts of several eV in energy mandatory.[20,21] These limitations of TD-DFT highlight the importance of having an accurate benchmark method that gives accurate absolute values combined with a balanced description of the spectra. Besides TD-DFT techniques, there are various methods available to describe core excitations more accurately. For example, the static-exchange[22] approach and

J. Wenzel, M. Wormit, A. Dreuw
Interdisciplinary Center for Scientific Computing, Ruprecht-Karls University, Im Neuenheimer Feld 368, 69120 Heidelberg, Germany
E-mail: jan.wenzel@iwr.uni-heidelberg.de or dreuw@uni-heidelberg.de
Contract grant sponsor: Deutsche Forschungsgemeinschaft "Forschergruppe 1789 Intermolecular and Interatomic Coulombic Decay"; Contract grant sponsor: Alexander von Humboldt foundation

the GW approximation to the Bethe–Salpeter equation,[23] as well as the coupled cluster singles and doubles[24–26] or the approximate coupled cluster scheme of second order (CC2).[27] The latter can be combined with a complex polarization propagator approach to obtain core excitation spectra directly.[28] For systems with large multireference character, a technique based on the multiconfiguration self-consistent-field approach is also available.[29]

In this work, we present results of our implementation[30] of the algebraic-diagrammatic construction scheme of second-order ADC(2)[31,32] for the calculation of core-excited electronic states. ADC is a well-known quantum chemical method for the calculation of excited states to study photochemistry of small and medium-sized molecules.[33,34] The overall accuracy for valence-excited states (UV region) of the strict version ADC(2)-s is 0.22 ± 0.5 eV, while the extended variant ADC(2)-x often underestimates the valence-excited states and exhibits an error of -0.7 ± 0.37 eV for standard organic molecules.[35] However, in contrast to TD-DFT, ADC is not hampered by SIE and thus has the capability to describe charge transfer and Rydberg states correctly.[19,36] The calculation of core-excited electronic states with ADC methods is nevertheless generally tedious, because the numerical solution of the ADC secular matrix eigenvalue problem is achieved via an iterative diagonalization procedure designed to yield the energetically lowest states of the excitation spectrum. As core-excited electronic states are located in the high-energy region of the spectrum (X-ray), they cannot be obtained directly unless the ADC matrix is fully diagonalized. This is computationally highly inefficient and practically not feasible for larger molecules. An elegant way to calculate these states is provided via the core-valence separation (CVS) approximation to the ADC working equations.[37–39] The basic idea of the CVS approximation relies on the large energetic separation between core and valence orbitals and on the strong localization of the core orbitals in space. Therefore, the interaction between core and valence-excited states can be neglected leading to a decoupling of the corresponding excitation spaces. Thereby, the diagonalization of the core excitation block becomes easily feasible.[37] A more detailed outline of the CVS approximation applied to the ADC method is given in the following section. As a large amount of energy is needed to promote an electron from the 1s core-level to the lowest unoccupied molecular orbital (LUMO) region, the resulting core hole leads to a strong localized spatial contraction of the electronic wavefunction, which can be understood as orbital relaxation. Within the CVS-ADC(2) method, these relaxation effects are included indirectly by means of double excitations, thus CVS-ADC(2)-x yields excellent results for core-excited states, as has been demonstrated previously.[40–42] Our new implementation of CVS-ADC(2) in the adcman program features a fully parallelized code for the calculation of closed-shell molecules using restricted Hartree–Fock (HF) molecular orbitals (MOs). The program exploits point group symmetry and delivers excitation energies and oscillator strengths for spin-pure singlet excited states as well as excitation energies of spin-pure triplet excited states.

The article is organized as follows. In the next section, a short outline of the CVS approximation applied to the ADC working equations is given. Afterward, a representative set of molecules from the field of organic electronics [acenaphthenequinone (ANQ), 3,4,9,10-perylentetracarboxylicacidianhydride (PTCDA), bithiophene (BT)] and biology (porphin, thymine) has been chosen to demonstrate the capabilities of our CVS-ADC(2) implementation and the accuracy of CVS-ADC(2) in the prediction of core excitation spectra of medium-sized molecules. Their calculated X-ray absorption spectra are discussed at the level of CVS-ADC(2)-x and compared with experimental data. At last, the results obtained at CVS-ADC(2)-s and CVS-ADC(2)-x levels of theory are compared with results computed using TD-DFT in combination with the B3LYP functional and with experimental values.

Theory and Implementation: The CVS Approximation Applied to ADC

A comprehensive derivation of the ADC formalism and the introduction of the CVS approximation has been given in previous literature.[31,32,37] An elegant route for the derivation of algebraic expressions of ADC schemes is provided via the intermediate state (IS) representation approach. Within this approach, the exact excited states are expanded in terms of a complete set of orthogonal orthonormalized IS $|\tilde{\Psi}_I\rangle$ that establish a matrix of the Hamiltonian shifted by the exact ground state energy E_0:

$$M_{IJ} = \langle \tilde{\Psi}_I | \hat{H} - E_0 | \tilde{\Psi}_J \rangle \tag{1}$$

This leads to the hermitian eigenvalue problem.

$$\mathbf{MX} = \mathbf{X\Omega}, \qquad \mathbf{X}^{\dagger}\mathbf{X} = \mathbf{1}. \tag{2}$$

where $\mathbf{\Omega}$ denotes the diagonal matrix of eigenvalues Ω_n and $\mathbf{X}$ is the matrix of eigenvectors. Consequently, diagonalization of the matrix $\mathbf{M}$ yields exact excitation energies Ω_n within the given basis set.

$$\Omega_n = E_n - E_0 \tag{3}$$

As neither the exact ground state wavefunction nor the exact ground state energy is generally known and the whole configuration space cannot be treated in an adequate computational time, one has to apply approximations. For ADC, Møller–Plesset perturbation theory [43] is used to describe the electronic ground state. The resulting ADC(2) and ADC(3) matrices consist of four different blocks: p-h,p-h; p-h,2p-2h; 2p-2h,p-h; and 2p-2h,2p-2h, which are treated in different orders of perturbation theory (Fig. 1). For ADC(2), two variants exist: in the strict version ADC(2)-s, the matrix elements of the 2p-2h/2p-2h block are expanded only in zeroth order, while in the extended variant ADC(2)-x they are expanded up to first order in perturbation theory. Explicit expressions for the matrix elements of $\mathbf{M}$ can be found elsewhere.[31,32] The eigenvectors of eq. (2) correspond to the transition amplitudes and give

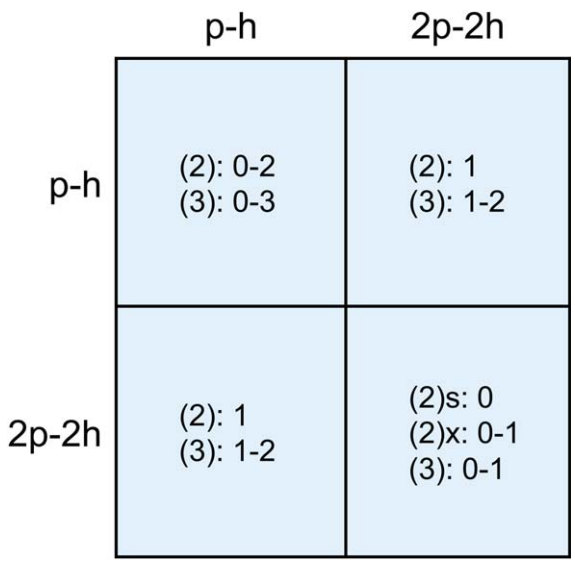

Figure 1. Structure of the ADC matrix ***M*** up to third order in perturbation theory. In every block, the order of terms contributing to this block at a specific overall order in perturbation theory is given. [Color figure can be viewed in the online issue, which is available at wileyonlinelibrary.com.]

access to properties like oscillator strengths and transition dipole moments.

Core-excited electronic states are located in the high-energy X-ray region of the electronic spectrum, while valence-excited states are energetically well separated and far below the core-level excitations. As typical iterative diagonalization schemes of the ADC matrix **M**, like for example the Davidson algorithm,[44] yield the energetically lowest eigenvalues, calculations of core-excited states with ADC methods are tedious: one has to compute all excited states energetically below the core excitations, which is computational unrealistic for systems with more than 10 electrons. Direct diagonalization of the core-excited space is in general prevented by couplings between valence and core-excited states. However, these couplings are very small (Fig. 2), because core orbitals are strongly localized in space and energetically well separated from the valence orbitals. This justifies the CVS approximation in which these couplings are neglected. Hence, the following types of Coulomb integrals practically vanish and can thus be set to exactly zero,

$$\begin{aligned} \langle Ip|qr\rangle = \langle pI|qr\rangle = \langle pq|Ir\rangle = \langle pq|rI\rangle = 0 \\ \langle IJ|pq\rangle = \langle pq|IJ\rangle = 0 \\ \langle IJ|Kp\rangle = \langle IJ|pK\rangle = \langle Ip|JK\rangle = \langle pI|JK\rangle = 0 \end{aligned} \quad (4)$$

where capital letters *I*, *J*, *K* refer to core orbitals and small letters *p*, *q*, *r* to valence orbitals. Discarding these couplings leads to a complete separation of singly core-valence-excited states from the valence-excited and doubly core-excited ones. Hence, the ADC matrix needs to be built only in the space of singly core-excited states and diagonalized leading to significant computational savings compared to the conventional ADC approach.

CVS-ADC(2) has been implemented in the adcman[30] program available in the Q-Chem[45] program package. To perform the tensor operations required to solve the ADC eigenvalue problem, adcman uses the newly developed general-purpose tensor library libtensor.[46] It provides the infrastructure for adcman to create tensors of arbitrary rank and size, and to perform linear algebra operations on them. The library is parallelized and fully supports symmetry, in particular spin and point group symmetry. Thereby, no special symmetry-adapted versions of the ADC equations are required to perform symmetry-aware calculations.

Within the implementation of the matrix-vector products for CVS-ADC, the index of the occupied orbital in the p-h configurations and one of the occupied indices in the 2p-2h configurations has to correspond to a core orbital. Therefore, only matrix elements corresponding to $M_{Ia,Jb}$ (p-h,p-h-block), $M_{Ijab,Kc}$ (2p-2h,p-h-block), $M_{Ia,Kjbc}$ (p-h,2p-2h-block), and $M_{Ijab,Klab}$ (2p-2h,2p-2h-block) need to be considered to obtain core-excited states, where *I*, *J*, and *K* represent core orbitals, while *j* and *l* describe occupied valence orbitals and *a*, *b*, *c*, and *d* virtual orbitals. For the calculation of transition moments, the transition density matrix form of the spectral amplitudes derived from the ADC formalism after applying the CVS approximation has been implemented, as well.

Finally, it should be noted that relativistic effects are not included within the CVS-ADC approach here. As core absorption spectra of light elements are not significantly influenced by relativistic effects and the contribution is only a positive shift of the absolute energy, they can be neglected.[39] However, the energy shift due to relativistic effects can be estimated to be about 0.1 eV for C 1s, 0.2 eV for N 1s, 0.4 eV for

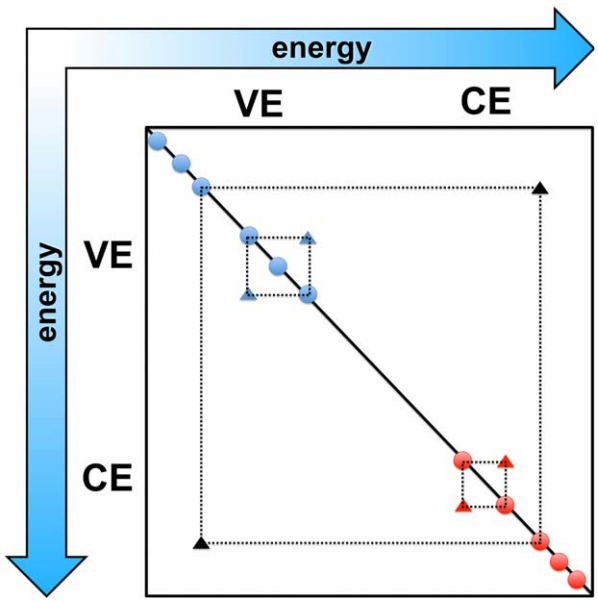

Figure 2. Schematic illustration of the core (CE, red) and valence (VE, blue) excited configurations for the p-h,p-h-block ordered by energy. The triangles represent couplings between the excited configurations. The black colored couplings between the CE and VE spaces prevent the direct diagonalization of the core-excited space.

O 1s, and 8.0 eV for S 1s excitations.[39,47] All computed values shown in this work are absolute without any level shift or consideration of relativistic effects.

Computational Details

Ground state geometry optimizations were performed with second-order Møller–Plesset perturbation theory (MP2)[43] using the def2-TZVPP[48] basis set in combination with the resolution-of-the-identity (RI)[49,50] approximation and the respective auxiliary TZVPP basis set, as this combination is known to provide accurate structures.[48,51–53] The only exception is the PTCDA molecule. Due to technical limitations, its ground state structure has been optimized at the level of DFT, using the B3LYP xc functional[54–56] and the def2-TZVPP basis set. All geometry optimizations have been performed with the TURBOMOLE 6.3.7 program.[57] To save computational time, the molecular point group symmetry has been exploited in the calculations of BT (C_2), ANQ (C_{2v}), porphin (D_{2h}), and PTCDA (D_{2h}). In case of the ANQ molecule, only the calculations of K-edge C 1s XAS spectra have been performed using C_{2v} point group symmetry, while the O 1s spectra have been computed without symmetry. Similarly, no point group symmetry has been exploited for the calculation of the thymine spectra, thereby demonstrating the capability of our implementation to disregard the symmetry of molecules, if required.

For the calculation of the core-excited states, our implementation of CVS-ADC(2)-s and CVS-ADC(2)-x as described above has been used. TD-DFT calculations of the core-excited states have been performed using the B3LYP xc functional as implemented in the ORCA 2.8 program.[58] To selectively obtain K-edge XAS spectra, only excitations from the respective 1s orbitals were included in the TD-DFT calculations.[59,60] The core-level excitation calculations have been performed using the 6–311++G**[61,62] basis set (thymine, BT, ANQ), the 6–31++G**[63–65] basis set (porphin), and the 6–31G**[63,64] basis set (PTCDA). It has been shown in the literature[4,40,66,67] that these basis sets provide precise results due to the polarization and diffuse functions that are needed to describe the core-excited states accurately. In case of porphin, the optically allowed B_{1u} core-excited states have also been computed using the larger 6–311++G** basis set to show that the deviations in the results are mostly due to basis set incompleteness. Due to technical reasons, the CVS-ADC(2) results are computed using the cartesian 6D/10F version of the respective basis sets, while the TD-DFT calculations are performed using the pure 5D/7F versions. However, the influence of the additional cartesian *d* and *f* polarization orbitals to the results obtained at the TD-DFT level should be relatively small compared to the inherent SIE.

Former work has shown that the computed oscillator strengths at the level of CVS-ADC(2)-x are in good agreement with experimentally measured intensities.[4,39,40,66,67]

X-Ray Absorption Spectra Calculated with the CVS-ADC(2)-x Method

In this section, we present the capabilities of our CVS-ADC(2)-x implementation by means of its application to a representative set of medium-sized molecules: at first, molecules used in the context of organic electronics (ANQ, BT, PTCDA) and then the biological relevant molecules thymine and porphin (see Fig. 3). It should be noted that the characterization of the core-excited states is done by means of the MO configurations using the MO expansion coefficients. As an electronic excited state in terms of ADC(2) is represented by combinations of singly and doubly excited configurations, there is often no single dominant configuration that is able to describe the actual excited state sufficiently. Furthermore, the larger the number of constituting atoms of a molecule, the higher is the density of core-excited states within a small energy region. Thus, to keep a clear view, only spectroscopically relevant bright core-excited states with their main MO contribution are given in most cases. Furthermore, only pictures of relevant MOs are presented.

Molecules in the field of organic electronics

Electronic devices based on organic materials like photovoltaic cells or organic light emitting devices are of high interest to the current applied research.[68–72] XAS helps to understand the charge transport mechanisms depending on intermolecular interactions, which are correlated with the electronic structure and the levels of the LUMOs of the molecules.[3] In principle, there are two types of molecules needed for any kind of organic electronic devices: electron donors and electron acceptors. Perylene derivatives like PTCDA and ANQ have been recognized as good acceptor molecules, while thiophenes are widely used as electron donors.[72–77] Therefore, we have selected ANQ, PTCDA, and BT (Fig. 3) to demonstrate the potential of CVS-ADC(2)-x calculations in the field of organic electronics.

X-ray absorption spectra of ANQ. ANQ is a medium-sized molecule with 20 atoms and, as it is a smaller related version of PTCDA, it represents a model system for electron acceptor molecules in organic electronic devices. Here, we compute the O 1s spectrum as well as the C 1s spectrum. Illustrations of the relevant MOs are given in Figure 4.

The CVS-ADC(2)-x results of the O 1s excitations are shown in Table 1 together with the experimental peak positions. As there is only one broad experimental peak in the low O 1s excitation energy domain between 529.2 and 531.4 eV, only the first eight core-excited states are shown. Due to the implicit C_{2v} symmetry, which has not been exploited in this calculation, the first eight core-excited states are pairwise degenerate. In case of the singlet states, each pair consists of one state which exhibits oscillator strength, while the other is almost optically forbidden. The CVS-ADC(2)-x result with 529.45 eV is very close to this experimental value exhibiting an error of 0.85 eV. The relative error is approximately 0.1% which is much smaller compared to the general relative error of ADC(2) for valence-excited states. The bright transition is mainly characterized by 51.7% of an electron promotion from a linear combination of the two O 1s orbitals to the π_3^* (LUMO+2) orbital. While the LUMO is mainly localized on the carbon system, the π_3^*-orbital has in addition a strong π^*

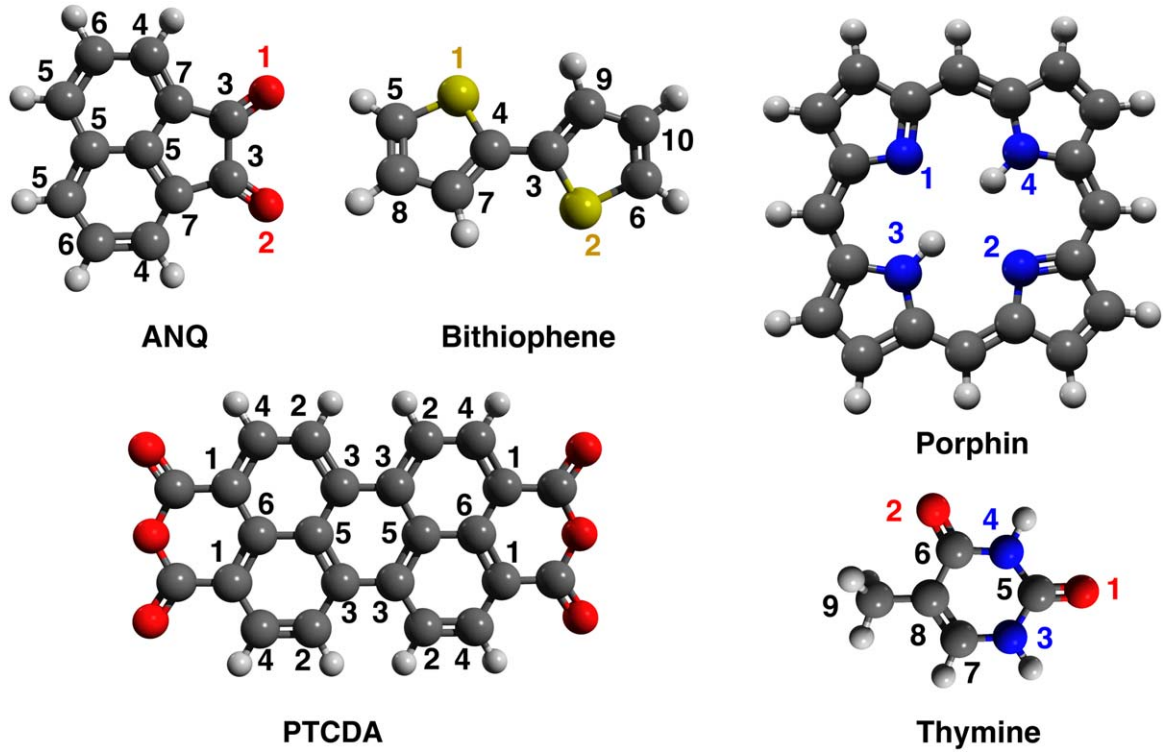

Figure 3. Structures of ANQ, PTCDA, BT, porphin, and the DNA base thymine. Elements are colored as gray (carbon), red (oxygen), blue (nitrogen), yellow (sulfur), and white (hydrogen). In case of ANQ and PTCDA, the atoms are numbered in groups. Each group consists of equivalent atoms whose 1s orbitals form the respective linear combinations of electron donor orbitals.

fraction located on the oxygen atoms. Hence, a significant overlap with the O 1s orbitals exists, resulting in a strong oscillator strength of 0.0689. The ratio of double excitations contributing to this state is considerable with 23%. Thus, the state features strong relaxation effects that are included via the double excitations. It should be noted, that all states are almost doubly degenerate, because of the C_{2v} symmetry of the system. Triplet states are also included in Table 1 to demonstrate that our implementation is capable of calculating such states in general.

As next step, the calculated C 1s spectrum of ANQ is presented. The CVS-ADC(2)-x results are compiled in Table 2. Henceforward, we neglect the triplet states, because they do not contribute to the absorption spectra. Within the first 18 core-excited states, only sπ*-states are found. The amount of doubly excited amplitudes contributing to each of these states ranges from 24% to 28%. Some states are doubly degenerated depending on the position of the donor carbon atoms related to the C_{2v} symmetry. Among them all optically allowed states are of B_2 symmetry. The energy of the first bright core-excited state 1 $^1B_2$ is only 0.3 eV larger than the experimental value of 284.1 eV, and the relative error is, therefore, 0.1%. This excitation is dominated by an electron promotion from the C7 atoms to the π_1^* and π_3^* virtual orbitals (see Figs. 3 and 4). The second experimentally observed peak is a mixture of the bright 2 $^1B_2$ and 3 $^1B_2$ states which are also dominated by a

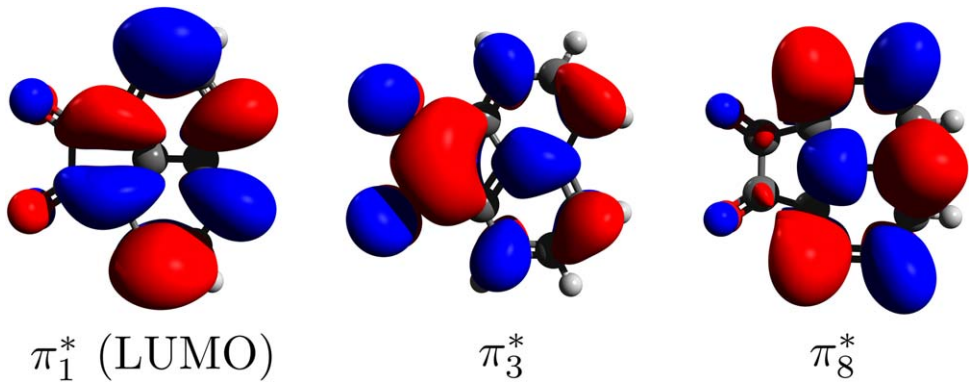

Figure 4. Illustration of the relevant virtual MOs (isovalue = 0.02) of ANQ at the level of HF/6–311++G**. [Color figure can be viewed in the online issue, which is available at wileyonlinelibrary.com.]

Table 1. Excitation energies (ω_{ex}), oscillator strengths (f_{osc}), character and amount of double amplitudes ($R2$) of the first eight O 1s singlet and triplet excited states of ANQ calculated using CVS-ADC(2)-x/6-311++G**.

State	ω_{ex}[eV]	f_{osc}	Main transition (1s →)	$R2$ [%]	ω_{ex}[eV] (Expt.)
T_1	528.99	–	O1,O2 → π_3^*	21	
T_2	528.99	–	O1,O2 → π_3^*	21	
S_1	529.45	0.0002	O1,O2 → π_3^*	23	
S_2	529.45	0.0689	O1,O2 → π_3^*	23	529.2−531.4
S_3	533.08	0.0000	O1,O2 → π_1^*	27	
S_4	533.08	0.0003	O1,O2 → π_1^*	27	
T_3	533.09	–	O1,O2 → π_1^*	27	
T_4	533.09	–	O1,O2 → π_1^*	27	

The calculated values are compared with experimental data.[78] Only the main transitions are shown. The numbering of the atoms complies with Figure 3.

transition to the π_1^* and the π_3^* orbitals. But in this case, the C4 and C5 carbons are the donor atoms. Here, the difference between experiment and calculation is 0.36 eV. As the first bright state has an error of 0.3 eV, the calculated shift between the first two bright calculated core-excited states is in perfect agreement with the experiment. The third bright state 4 $^1B_2$ exhibits an error of 0.16 eV compared to the experiment, which is slightly lower than for the previous two states. This state is described by an excitation from the C6 carbons to the π_1^* and π_8^* orbitals. For the fourth bright core-excited state 5 $^1B_2$, which can be matched with the experimental value of 285.0 eV, the error of 0.27 eV is again of similar magnitude as the one of the first two peaks. The same applies for the fifth bright experimental state of interest at 285.6 eV, which is a broad peak and a mixture of different core-excited states (see Table 2). The calculated values range from 285.6 to 285.92 eV. The highest oscillator strength among these states stems from the degenerate states 8 $^1B_2$ and 9 $^1B_2$, exhibiting an error to the experiment of 0.32 eV. In summary, all excitation energies calculated with CVS-ADC(2)-x show an almost constant absolute and very small relative error and are in almost perfect agreement with the experimental spectrum, in particular, when considering the errors due to the neglected relativistic effects. Only the third bright state is an exception exhibiting a smaller difference to experiment of 0.16 eV.

X-ray absorption spectra of BT. Thiophene derivatives are often used as electron donors in the field of organic solar cells, because they feature strong absorption bands in the UV region and corresponding fluorescence properties which lead in combination with appropriate energy and electron acceptors to high-energy transfer quantum yields as well as high charge transfer rates.[72,77,79] Hence, BT has been selected as second representative example. Figure 5 shows the relevant virtual orbitals of BT in the 6-311++G** basis set. It should be noted that due to the strong polarized and diffuse basis set, the orbitals d_1^*, d_2^*, d_{10}^*, and d_{18}^* do not have a clear π^*-character, because they are dominated by the diffuse functions showing the characteristics of an additional weakly bound electron rather than an excited electron. Nevertheless, the

Table 2. Excitation energies (ω_{ex}), oscillator strengths (f_{osc}), character and amount of double amplitudes ($R2$) of the first 18 C 1s singlet excited states of ANQ calculated using CVS-ADC(2)-x/6-311++G** exploiting C_{2v} point group symmetry.

State	ω_{ex}[eV]	f_{osc}	Main transition (1s →)	$R2$ [%]	ω_{ex}[eV] (Expt.)
1 $^1A_2$	284.40	0.000	C7 → π_1^*, π_3^*	26	284.1
1 $^1B_2$	284.40	0.038	C7 → π_1^*, π_3^*	26	
2 $^1A_2$	284.78	0.000	C4 → π_1^*, π_3^*	25	
2 $^1B_2$	284.78	0.041	C4 → π_1^*, π_3^*	25	
3 $^1A_2$	284.81	0.000	C5 → π_1^*, π_3^*	25	284.45
3 $^1B_2$	284.81	0.086	C5 → π_1^*, π_3^*	25	
4 $^1A_2$	284.96	0.000	C6 → π_1^*, π_8^*	26	
4 $^1B_2$	284.96	0.036	C6 → π_1^*, π_8^*	26	284.8
5 $^1B_2$	285.27	0.024	C5 → π_3^*, π_8^*	24	285.0
5 $^1A_2$	285.42	0.000	C5 → π_1^*	28	
6 $^1A_2$	285.47	0.000	C5 → π_1^*	28	
7 $^1A_2$	285.60	0.000	C7 → π_3^*, π_1^*	27	
6 $^1B_2$	285.60	0.014	C7 → π_3^*, π_1^*	27	
7 $^1B_2$	285.74	0.028	C5 → π_3^*, π_8^*	25	
8 $^1A_2$	285.90	0.000	C3 → π_3^*, π_1^*	23	285.6
9 $^1A_2$	285.92	0.000	C6 → π_8^*, π_3^*	26	
8 $^1B_2$	285.92	0.034	C6 → π_8^*, π_3^*	26	
9 $^1B_2$	285.92	0.089	C3 → π_3^*, π_1^*	24	

The calculated values are compared with experimental data.[2] Only the main transitions are shown. The numbering of the atoms complies with Figure 3.

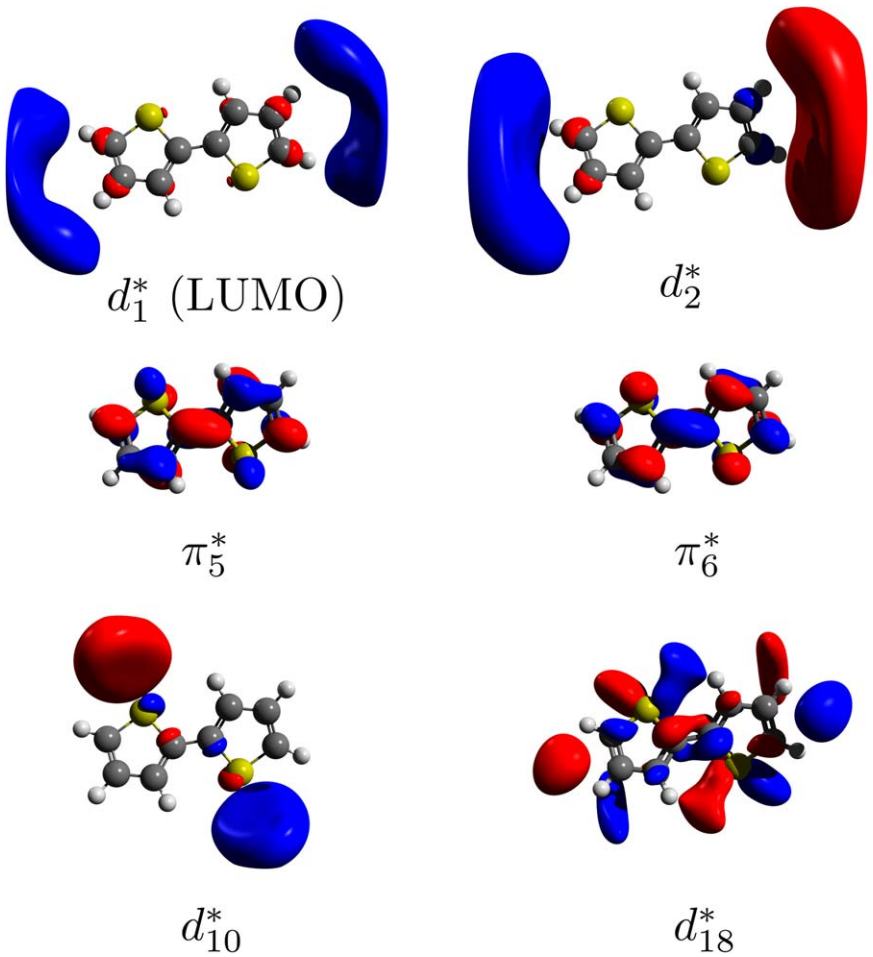

Figure 5. Illustration of the relevant virtual MOs (isovalue = 0.015−0.025) of BT at the level of HF/6–311++G**. [Color figure can be viewed in the online issue, which is available at wileyonlinelibrary.com.]

orbitals acting as main contributions to the bright excited states show a clear π^*-character and should be described reasonably well in any basis set. As shown in previous work,[72],[80–83] the BT molecule is not planar in the ground state, and the central dihedral angle (S1-C4-C3-S2) is −150.1° optimized at the level of RI-MP2 using the def2-TZVPP basis set resulting in C_2 point group symmetry.

Let us first take a look at the 1s core excitations of the sulfur atoms calculated with CVS-ADC(2)-x (Table 3). Similar to the O 1s spectrum of ANQ, only the first bright experimental peak at 2474 eV is discussed. At the level of CVS-ADC(2)-x this band is described as a mixture of the first four core-excited states which are pairwise degenerate due to the C_2 symmetry with excitation energies of 2468.83 and 2468.97 eV, respectively. The bright excitation is, therefore, underestimated by 5.1 eV, that is, 0.2%, compared to the experiment, which again corresponds approximately to the estimated magnitude of the missing relativistic effects. It should be noted that the experiments have been performed using crystal powder of oligothiophenes. Also, the donor orbitals of all transitions are ± linear

Table 3. Excitation energies (ω_{ex}), oscillator strengths (f_{osc}), character and amount of double amplitudes (*R*2) of the first six S 1s singlet excited states of BT calculated using CVS-ADC(2)-x/6-311++G** exploiting C_2 point group symmetry.

State	ω_{ex}[eV]	f_{osc}	Main transition (1s →)	*R*2 [%]	ω_{ex}[eV] (Expt.)
1 ^{1}B	2468.83	0.0057	S1,S2 → π_5^*, π_6^*	15	
1 ^{1}A	2468.83	0.0023	S1,S2 → π_5^*, π_6^*	15	
2 ^{1}B	2468.97	0.0057	S1,S2 → π_6^*, d_{18}^*	15	2474
2 ^{1}A	2468.97	0.0031	S1,S2 → π_6^*, d_{18}^*	15	
3 ^{1}A	2470.69	0.0001	S1,S2 → d_1^*, d_{10}^*	15	
3 ^{1}B	2470.69	0.0006	S1,S2 → d_1^*, d_{10}^*	15	

The calculated values are compared with experimental data of oligothiophenes (crystal powder).[6] Only the main transitions are shown. The numbering of the atoms complies with Figure 3.

Table 4. Excitation energies (ω_{ex}), oscillator strengths (f_{osc}), character and amount of double amplitudes ($R2$) of the first 14 C 1s singlet excited states of BT calculated using CVS-ADC(2)-x/6-311++G** exploiting C_2 point group symmetry.

State	ω_{ex}[eV]	f_{osc}	Main transition (1s $\rightarrow$)	$R2$ [%]	ω_{ex}[eV] (Expt.)
1 ^{1}B	285.19	0.004	C7–C10 $\rightarrow \pi_5^*, \pi_6^*$	26	
1 ^{1}A	285.19	0.041	C7–C10 $\rightarrow \pi_5^*, \pi_6^*$	26	
2 ^{1}B	285.42	0.008	C5,C6 $\rightarrow \pi_5^*, \pi_6^*$	26	
2 ^{1}A	285.42	0.115	C5–C6 $\rightarrow \pi_5^*, \pi_6^*$	26	285.7
3 ^{1}A	285.44	0.000	C5–C10 $\rightarrow \pi_5^*, \pi_6^*$	26	
3 ^{1}B	285.44	0.000	C5–C10 $\rightarrow \pi_5^*, \pi_6^*$	26	
4 ^{1}B	285.67	0.003	C3,C4 $\rightarrow \pi_5^*, \pi_6^*$	25	
4 ^{1}A	285.70	0.056	C3,C4 $\rightarrow \pi_5^*, \pi_6^*$	25	
5 ^{1}B	287.08	0.001	C7–C10 $\rightarrow \pi_5^*, \pi_6^*$	25	
5 ^{1}A	287.08	0.038	C7–C10 $\rightarrow \pi_5^*, \pi_6^*$	25	
6 ^{1}B	287.14	0.008	C7–C10 $\rightarrow d_1^*, d_2^*$	26	286.7
6 ^{1}A	287.14	0.003	C7–C10 $\rightarrow d_1^*, d_2^*$	26	
7 ^{1}A	287.19	0.000	C7–C10 $\rightarrow d_1^*, d_2^*$	26	
7 ^{1}B	287.19	0.010	C7–C10 $\rightarrow d_1^*, d_2^*$	26	

The calculated values are compared with experimental data of BT monolayer adsorbed on a Ag(111) surface.[84] Only the main transitions are shown. The numbering of the atoms complies with Figure 3.

combinations of the two sulfur 1s orbitals as a result of the C_2 symmetry. The first two transitions are dominated by an electron promotion to the π_5^* and π_6^* orbitals, while the two next higher states are best described by transitions to the π_6^* and d_{18}^* orbitals. All of these virtual orbitals are delocalized over the whole BT molecule and with the exception of d_{18}^* have a distinct π*-character (see Fig. 5). The amount of double amplitudes contributing to the states is 15% which indicates that relaxation effects are less important within the S 1s excitations of BT than within the O 1s and C 1s excitations of ANQ for which the double amplitudes amount to about 25% (Tables 1 and 2).

Next, the C 1s spectrum of the BT molecule will be discussed (Table 4). The first two experimental peaks of the C 1s spectrum are compared to the results of the CVS-ADC(2)-x method. It should be noted that the experiments are performed with BT molecules adsorbed on a Ag(111) surface, while the calculations do not consider environmental influences. Again, the C_2 point group symmetry leads to doubly degenerate states in most of the cases. The first experimental peak at 285.7 eV can be described as a superposition of the first eight core-excited states. The energy ranges from 285.19 to 285.70 eV, with the 2 ^{1}A state having the largest oscillator strength of 0.115 at 285.42 eV. Therefore, the first core-excited experimental peak is slightly underestimated by about 0.3 eV with a very small relative error of only 0.1%. All eight states contributing to the first peak are characterized as transitions to the π_5^* and π_6^* orbitals including linear combinations of all eight carbon 1s orbitals as donor orbitals. This is similar to the S 1s spectrum. The amount of double amplitudes contributing to these states is between 25% and 26% hinting toward important relaxation effects. The second experimental peak at 286.7 eV can again be assigned to a mixture of six states with excitation energies from 287.08 to 287.19 eV. The highest oscillator strength of 0.038 belongs to the state 5 ^{1}A resulting in an absolute error of 0.38 eV compared to the experiment. All of these six states can be characterized as transitions from the linear combinations of the C7, C8, C9, and C10 1s orbitals to the $\pi_{5,6}^*$ and $d_{1,2}^*$ orbitals. Again, relaxation effects of the electronic wavefunction are important as indicated by the large amount of double amplitudes of around 25%. In contrast to the first bright excitation, the energy of this state is slightly overestimated. Therefore, the experimental energy gap of these first two peaks of 1 eV is computed to be 1.66 eV at the CVS-ADC(2)-x level, which may still be acceptable taking into account the lack of the Ag surface interactions.

X-ray absorption spectrum of PTCDA. PTCDA is a dark red pigment and its derivatives or nitrogen variants like MePTCDI are often used in organic solar cells and organic semiconductors, as their electronic structures allow them to serve as electron acceptor.[72,77,79] In Figure 6, the relevant MOs for the core-excited states are shown. The CVS-ADC(2)-x results for the C 1s excitations using D_{2h} point group symmetry are given in Table 5. As its molecular size with 38 atoms is quite large, the smaller 6-31G** basis set had to be used. Based on spectroscopic selection rules, only states belonging to the irreducible representations B_{1u}, B_{2u}, and B_{3u} are one photon allowed and can have oscillator strength. In general, B_{1u} states exhibit significantly larger oscillator strengths than the others, thus only the first eight B_{1u} states will be discussed.

According to our calculations, the first experimental peak at 284.4 eV is composed of a mixture of the first four core-excited B_{1u} states with energies ranging from 285.36 to 285.75 eV. The 4 $^1B_{1u}$ state has the largest oscillator strength with 0.090 relating to an absolute error in excitation energies of 1.35 eV (0.5%) compared to the experiment. The larger relative error compared to the ANQ and BT results is most likely due to the smaller basis set used for the PTCDA calculation. The states contributing to the first peak are characterized as transitions to the LUMO and LUMO+2 including 26–27% double amplitudes. The donor MOs are linear combinations of the 1s orbitals of the carbon atoms C1–C4. For a better overview, the carbon atoms are collected in groups according to the D_{2h}

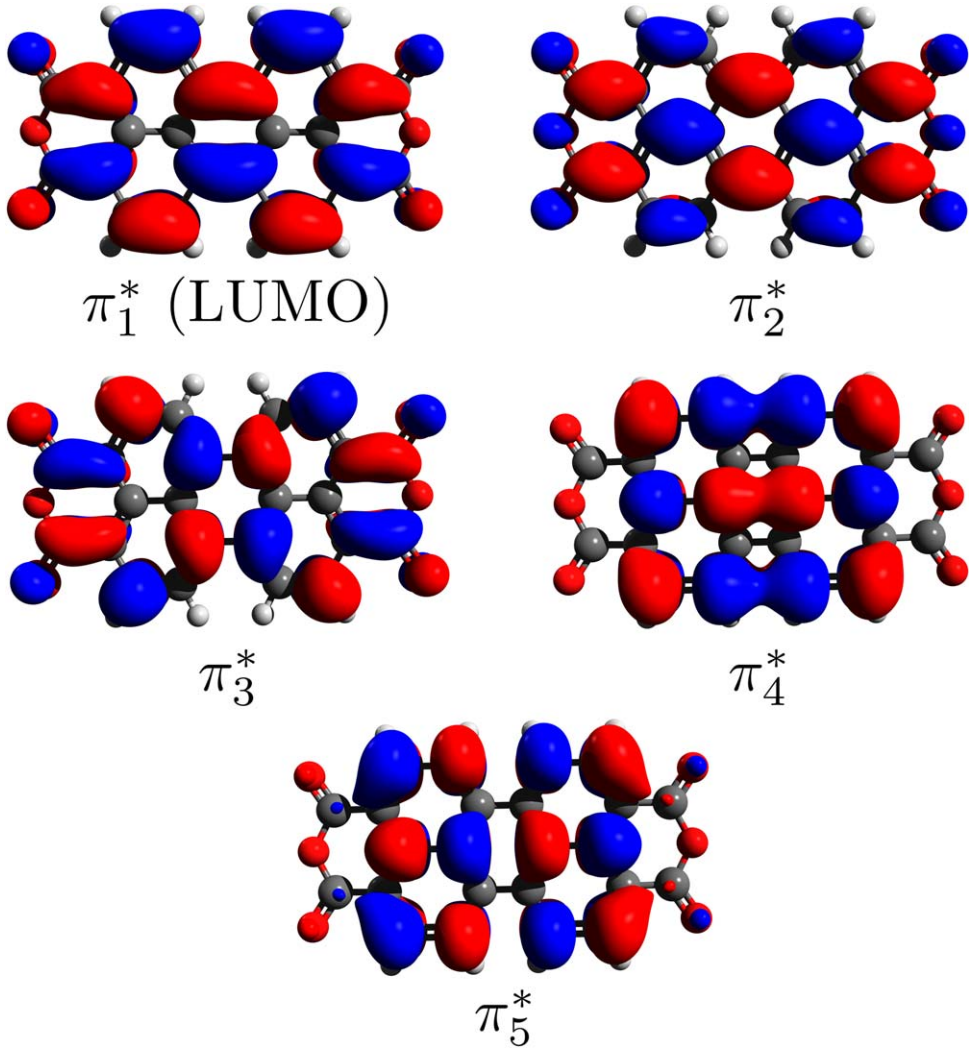

Figure 6. Illustration of the relevant virtual MOs (isovalue = 0.02) of PTCDA at the level of HF/6–31G**. [Color figure can be viewed in the online issue, which is available at wileyonlinelibrary.com.]

symmetry (see Fig. 3). The second experimental peak comprises the four next higher B_{1u} states with the largest oscillator strength of 0.095 for the 7 $^1B_{1u}$ state. Thus, the error with respect to the experiment amounts to about 1.63 eV (0.6%). Here, the transitions are dominated by electron promotions from C2, C4, C5, and C6 to the first five virtual orbitals (π_1^*–π_5^*). The amount of doubles is again large with 22–26% calling for strong relaxation effects. However, the use of smaller less diffuse basis sets, here 6-31G**, results in larger relative errors than in case of the more diffuse basis set, 6-311++G** used before, but the peak structure of the experimental spectrum is still very well reproduced.

Biologically relevant molecules

Porphin has been chosen as a representative molecule of interest in both organic electronics and biology. Porphin and porphyrine derivatives are used in chemical sensors, as well as they are studied to understand energy transfer processes in photosynthetic systems.[85,86] Their biological relevance is demonstrated as building blocks in the oxygen transport center of hemoglobin or as light-harvesting pigments in photosynthetic proteins, just to mention a few examples. We have further investigated the DNA nucleobase thymine to augment earlier CVS-ADC(2) studies[40] of this molecule which have been performed with a small basis set. For testing purposes, we have recomputed the core-excited states of thymine with a larger and more diffuse basis set. As recent research in cancer therapy concentrates on low-energy electron generation via ICD after a resonant core excitation, nucleobases are a potential target.[14,15] The structures of porphin and thymine are shown in Figure 3.

X-ray absorption spectra of thymine. As K-shell absorption spectra of thymine calculated with the CVS-ADC(2)-x method have already been discussed in detail in previous work, we concentrate here on the improvement of the results using a larger 6-311++G** basis set including two sets of diffuse and polarization functions, while before only the small 6-31+G basis set had been used. The former work also provides a comparison of the computed oscillator strengths with the experimentally measured intensities. The calculated oscillator

Table 5. Excitation energies (ω_{ex}), oscillator strengths (f_{osc}), character and amount of double amplitudes ($R2$) of the first eight B_{1u} C 1s singlet excited states of PTCDA calculated using CVS-ADC(2)-x/6-31G** exploiting D_{2h} point group symmetry.

State	ω_{ex}[eV]	f_{osc}	Main transition (1s $\rightarrow$)	$R2$ [%]	ω_{ex}[eV] (Expt.)
1 $^1B_{1u}$	285.36	0.072	C1 $\rightarrow \pi_1^*, \pi_3^*$	26	
2 $^1B_{1u}$	285.44	0.058	C2 $\rightarrow \pi_1^*$	27	284.4
3 $^1B_{1u}$	285.72	0.073	C3 $\rightarrow \pi_1^*$	26	
4 $^1B_{1u}$	285.75	0.090	C4 $\rightarrow \pi_1^*, \pi_3^*$	26	
5 $^1B_{1u}$	287.11	0.061	C5 $\rightarrow \pi_2^*, \pi_4^*$	23	
6 $^1B_{1u}$	287.19	0.090	C2 $\rightarrow \pi_4^*, \pi_5^*, \pi_3^*$	25	285.6
7 $^1B_{1u}$	287.23	0.095	C6 $\rightarrow \pi_4^*, \pi_5^*, \pi_2^*$	22	
8 $^1B_{1u}$	287.30	0.076	C4 $\rightarrow \pi_4^*, \pi_5^*, \pi_1^*$	26	

The calculated values are compared with experimental data.[2] Only the main transitions are shown. The numbering of the atoms complies with Figure 3.

strengths are in a good agreement to experimental intensities and relatively independent of the size of the basis set. In Table 6, the first 15 C 1s states calculated at the CVS-ADC(2)-x level are listed.

Generally, the results can be summarized by three important statements. Most importantly, the relative error in these excitation energies is reduced from about 1%, that is, approximately 2.5 eV, to only 0.2%, that is, at most 0.65 eV, when the larger basis set is used. The order of the states changes slightly. However, oscillator strengths do not differ much between the two basis sets. As a consequence of the larger basis set, no shifting of the computed excitation energies is necessary to achieve agreement with the experiment. These findings demonstrate the basis set dependence of the CVS-ADC(2)-x method. Generally, the ADC formalism provides a balanced description of electron correlation in both ground and excited state that leads to cancellation of errors in the excitation energies. Furthermore, neglecting relativistic contributions to the K-shell excitations reduce the error produced at the level of CVS-ADC(2)-x/6–311++G**. Taking into account the computed results of ANQ and BT, the combination of the CVS-ADC(2)-x with the 6–311++G** basis set potentially provides a fortuitous error compensation of electron correlation, orbital relaxation, basis set dependence, and relativistic effects resulting in core excitation energies close to experiment.

Let us now turn to the N 1s spectrum of thymine (Table 7). Here, the first two bright experimental peaks are evaluated. The findings are similar to the C 1s results. Using the smaller 6-31+G basis set leads to a relative error of 0.59–0.69%, which corresponds to an absolute error of 2.36–2.79 eV. Using the larger basis set reduces the error to less than 0.1%, that is, 0.2 eV. While a constant shift of about 2.6 eV had to be applied to the excitation energies obtained with the smaller basis set, the CVS-ADC(2)-x calculations with the larger 6-311++G** basis set exhibit again a remarkable agreement with the experiment.

Analysis of the O 1s spectrum of thymine (Table 8) reveals that the relative error is 0.31%–0.42% with the smaller basis set relating to an absolute error of about 2.2 eV. Our calculations with the 6-311++G** basis set reveal an underestimation of only 0.76–1.56 eV (0.14%–0.29%), and are, therefore, closer to the experimental values. Especially, the energy

Table 6. Excitation energies (ω_{ex}), oscillator strengths (f_{osc}), and relative errors of the first 15 C 1s singlet excited states of thymine calculated using CVS-ADC(2)-x.

	Previous work			Our work			Expt.
State	ω_{ex}[eV]	f_{osc}	Error [%]	ω_{ex}[eV]	f_{osc}	Error [%]	ω_{ex}[eV]
1	287.02	0.024	0.74	284.84	0.024	−0.02	284.9
2	288.54	0.045	0.92	286.36	0.045	0.16	285.9
3	288.97	0.000		286.90	0.000		
4	289.05	0.004		287.11	0.003		
5	289.38	0.000		287.29	0.000		
6	289.98	0.007		287.95	0.015	0.23	287.3
7	290.06	0.015	0.96	288.03	0.007		
8	290.23	0.001		288.07	0.002		
9	290.37	0.007		288.24	0.053	0.15	287.8
10	290.40	0.013		288.34	0.000		
11	290.42	0.056	0.91	288.39	0.004		
12	290.46	0.000		288.45	0.013	0.02	288.4
13	290.62	0.000		288.63	0.000		
14	290.95	0.010	0.88	288.88	0.008		
15	291.00	0.001		289.11	0.002		

The calculated values are compared with experimental data and previous work.[40] Our calculations have been performed using the 6–311++G** basis set, while in the previous work the 6–31+G basis set had been used.

Table 7. Excitation energies (ω_{ex}), oscillator strengths (f_{osc}), and relative errors of the seven energetically lowest N 1s singlet excited states of thymine calculated using CVS-ADC(2)-x.

	Previous work			Our work			Expt.
State	ω_{ex}[eV]	f_{osc}	Error [%]	ω_{ex}[eV]	f_{osc}	Error [%]	ω_{ex}[eV]
1	404.06	0.0119	0.59	401.50	0.0111	−0.05	
2	404.43	0.0085		401.82	0.0070		401.7
3	404.61	0.0079		402.21	0.0078		
4	405.03	0.0069		402.54	0.0035		
5	405.11	0.0035		402.60	0.0066		402.7
6	405.49	0.0098	0.69	403.03	0.0106	0.08	
7	405.91	0.0055		403.42	0.0050		

The calculated values are compared with experimental data and previous work.[40] Our calculations have been performed using the 6–311++G** basis set, while in the previous work the 6–31+G basis set had been used.

difference between the first two experimental peaks that are properly described by the first two calculated bright states are perfectly reproduced by CVS-ADC(2)-x with both basis sets. Although CVS-ADC(2)-x benefits largely from the fortuitous error compensation as outlined above, the remaining error has about the size of the neglected relativistic effects.

Nitrogen 1s X-ray absorption spectrum of porphin. As last representative example, we have chosen to study the core-excited states of porphin. Here, the core excitations from the nitrogen 1s orbitals have been calculated. Relevant MOs are illustrated in Figure 7. Due to the polarized and diffuse functions of the 6-311++G** basis set, extremely diffuse unoccupied MOs occur in the low-energy regime, like d^*_{16} and d^*_{19}, which correspond more to weakly bound additional electrons. As the calculation is performed using D_{2h} point group symmetry, only excited states with the irreducible representations B_{1u}, B_{2u}, and B_{3u} are optically allowed and can have oscillator strength. Similar to the PTCDA molecule above, the B_{1u} states have much larger oscillator strengths than the others and hence, we focus here on the B_{1u} states only. The CVS-ADC(2)-x results are summarized in Table 9. Again, the influence of the larger 6–311++G** basis set on the excitation energies of the B_{1u} states is readily apparent.

Comparison with the experimental core excitation spectrum obtained from a solid film of porphin, reveals that the first experimental peak at 398.2 eV is perfectly reproduced by CVS-ADC(2)-x using the larger basis set. The absolute error is tiny with only 0.03 eV, while use of the smaller double-zeta 6–31++G** basis set leads already to an error of 1.69 eV. This points again to the fortuitous cancellation of errors in the used CVS-ADC(2)-x/6–311++G** approach. The same trend holds for the 2 $^1B_{1u}$ state, which corresponds to the second peak of the experimental spectrum. Here, the absolute error obtained with the large basis set is only 0.05 eV, while the smaller basis yields an error of 1.82 eV. The energy difference between these states is well described with both basis sets. Analysis of the involved MOs shows that the 1 $^1B_{1u}$ state is characterized by an electron promotion from a linear combination of the N 1s orbitals located on the deprotonated

Table 8. Excitation energies (ω_{ex}), oscillator strengths (f_{osc}), and relative errors of the first 15 O 1s singlet excited states of thymine calculated using CVS-ADC(2)-x.

	Previous work			Our work			Expt.
State	ω_{ex}[eV]	f_{osc}	Error [%]	ω_{ex}[eV]	f_{osc}	Error [%]	ω_{ex}[eV]
1	533.55	0.0310	0.40	530.52	0.0282	−0.17	531.4
2	534.53	0.0293	0.42	531.54	0.0268	−0.14	532.3
3	536.52	0.0001		533.30	0.0001		
4	536.67	0.0004		533.43	0.0003		
5	536.97	0.0002		533.73	0.0003		
6	537.32	0.0016		534.10	0.0012		
7	537.35	0.0026	0.31	534.14	0.0027	−0.29	
8	537.47	0.0000		534.20	0.0002		
9	537.73	0.0020		534.37	0.0013		
10	537.75	0.0006		534.56	0.0006		535.7
11	537.80	0.0019		534.71	0.0019		
12	538.09	0.0011		534.77	0.0007		
13	538.17	0.0011		534.90	0.0009		
14	538.33	0.0020		534.94	0.0018		
15	538.60	0.0001		535.26	0.0001		

The calculated values are compared with experimental data and previous work.[40] Our calculations have been performed using the 6–311++G** basis set, while in the previous work the 6–31+G basis set had been used.

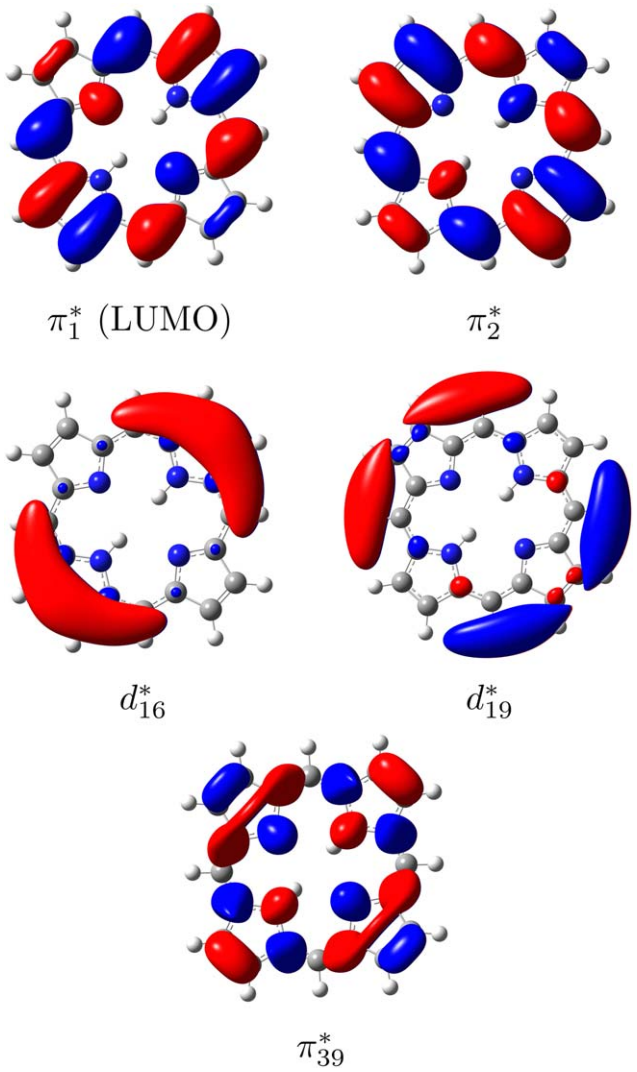

Figure 7. Illustration of the relevant virtual MOs (isovalue = 0.02) of porphin at the level of HF/6–311++G**. [Color figure can be viewed in the online issue, which is available at wileyonlinelibrary.com.]

nitrogens to the π_1^*, while the 2 $^1B_{1u}$ state is dominated by a transition to the π_2^* with the 1s orbitals of the protonated nitrogens as electron donor. The amount of double amplitudes is large with 26% and 25%, respectively, indicating strong relaxation effects. The third and fourth experimental peaks are not well resolved as they are included in a broad absorption band. According to our calculations, the third experimental peak at 402.3 eV can be described as a mixture of 3 $^1B_{1u}$ and 4 $^1B_{1u}$. The excitation energies of these states are underestimated by 1.12 and 0.57 eV, respectively, using the triple-zeta 6–311++G** basis set. The amount of double amplitudes is 26% and the transition is characterized as excitations of the deprotonated nitrogen into the π_{39}^*, d_{16}^*, and d_{19}^* MOs. Owing to the larger error in the computed third peak than in the second one, the energy difference between these states is only 0.83 eV at CVS-ADC(2)-x/6–311++G** level instead of the experimental value of 2 eV. The fourth peak at 403.9 eV in the experiment is, however, again well described. The calculated excitation energies using the large basis set is 403.37 eV, exhibiting an error of only 0.53 eV. Within the orbital picture, the main transition can be characterized as an electron promotion from the protonated nitrogen 1s orbitals to the π_{39}^* and d_{16}^* MOs. However, as the experimental spectrum of the solid species features a broad absorption including peak three and four, the error analysis of the calculated values should be taken with a grain of salt, in particular, because the calculations are performed in vacuum. The 1 $^1B_{1u}$ and 2 $^1B_{1u}$ states are well defined in the experimental spectrum and can be properly assigned by our calculations.

Comparison of CVS-ADC(2) to TD-DFT

In this section, the previously discussed results of the CVS-ADC(2)-x calculations are compared to CVS-ADC(2)-s, as well as to TD-DFT/B3LYP results, as TD-DFT has proven now several times to yield quite accurate results for core excitation spectra, in particular in combination with the B3LYP functional. [21,87–89] Figure 8 summarizes the arithmetic mean errors of the computed excitation energies with respect to experimental values for all three methods, which have been evaluated for each molecule and every core excitation separately. As example, the results for the ANQ molecule are analyzed here (Tables 10 and 11). Tables containing the data of the detailed comparison

Table 9. Excitation energies (ω_{ex}), oscillator strengths (f_{osc}), character, and amount of double amplitudes (*R*2) of the first eight B_{1u} C 1s singlet excited states of porphin calculated using CVS-ADC(2)-x exploiting D_{2h} point group symmetry.

	6–31++G**		6–311++G**				Expt.
State	ω_{ex}[eV]	f_{osc}	ω_{ex}[eV]	f_{osc}	*R*2 [%]	Main transition (1s →)	ω_{ex}[eV]
1 $^1B_{1u}$	399.89	0.0338	398.07	0.0351	26	N1,N2 → π_1^*	398.2
2 $^1B_{1u}$	402.12	0.0268	400.35	0.0280	25	N3,N4 → π_2^*	400.3
3 $^1B_{1u}$	403.03	0.0263	401.18	0.0257	26	N1,N2 → π_{39}^*	402.3
4 $^1B_{1u}$	403.59	0.0079	401.73	0.0095	26	N1,N2 → $\pi_{16}^*, d_{19}^*, \pi_{39}^*$	
5 $^1B_{1u}$	404.29	0.0012	402.47	0.0011	27	N1,N2 → $d_{19}^*, \pi_{24}^*, \pi_{23}^*$	
6 $^1B_{1u}$	404.82	0.0019	402.97	0.0027	27	N1,N2 → π_{23}^*, d_{16}^*	
7 $^1B_{1u}$	404.90	0.0008	403.08	0.0003	27	N1,N2 → $\pi_{26}^*, d_{19}^*, \pi_{24}^*$	
8 $^1B_{1u}$	405.18	0.0187	403.37	0.0178	25	N3,N4 → π_{39}^*, d_{16}^*	403.9
9 $^1B_{1u}$	405.37	0.0001	403.51	0.0001	27	N1,N2 → π_{24}^*, π_{23}^*	
10 $^1B_{1u}$	405.74	0.0085	403.91	0.0005	27	N1,N2 → $\pi_{35}^*, \pi_{60}^*, \pi_{39}^*$	

The calculated values are compared with experimental data of a solid porphin film.[86] Only the main transitions are shown. The numbering of the atoms complies with Figure 3. The calculations have been performed using the 6–31++G** and 6–311++G** basis sets.

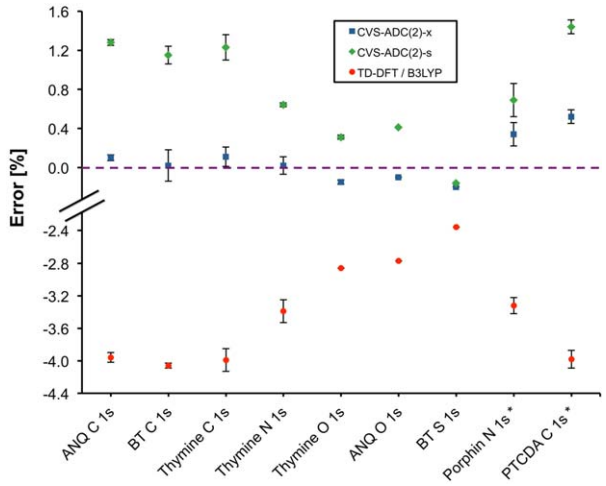

Figure 8. Graphical representation of the calculated relative arithmetic mean errors of the excitation energies compared to experimental values. The means are calculated for each type of core excitation and every molecule using all excitations of the respective type that can be assigned to experimental data. The dashed line indicates a discrepancy of 0% to the experiment. The vertical bars illustrate the standard deviation. It should be noted that the values marked with a * are not directly comparable to the rest, because smaller basis sets have been used for these calculations. [Color figure can be viewed in the online issue, which is available at wileyonlinelibrary.com.]

between TD-DFT and CVS-ADC(2)-s and -x calculations for the other molecules are listed and discussed in the Supporting Information.

Starting with the results for the O 1s core excitations of ANQ, comparison with experiment shows that B3LYP underestimates the fourth lowest bright core-excited state by ~14.3 eV (relative error 2.8%), while CVS-ADC(2)-s overestimates its excitation energy by ~2.2 eV (relative error 0.4%). This bright singlet state has 23% of double excitation character at the CVS-ADC(2)-x level, while CVS-ADC(2)-s yields only 18%. With an error of only 0.85 eV (0.1%), CVS-ADC(2)-x exhibits the most accurate result of the investigated methods. Comparing the three methods, the first four states are in identical order, while the subsequent states exhibit a slightly different order due to the small energy differences between them ($\Delta\omega \leq 0.02$ eV $\sim 7 \cdot 10^{-4}$ au), which are close to the diagonalizer convergence threshold.

The comparison of the ANQ C 1s excitation spectra calculated at the three levels of theory (Table 11) yields a similar picture as for the O 1s one. It is noticeable that the number of states matching an experimental peak varies between the methods. For example, the third experimental peak is described by one bright state using the CVS-ADC(2)-x method, while B3LYP and CVS-ADC(2)-s yield two states contributing to this peak. Compared to the O 1s result the relative error of the first bright state calculated with TD-DFT/B3LYP is with 4.0% considerably larger, as is the relative error of CVS-ADC(2)-s with 1.3%. The absolute errors between the calculated states and the experimental values at TD-DFT/B3LYP level are essentially constant with values ranging from 10.6 to 11.0 eV. Therefore, by addition of an absolute, constant energy shift to the TD-DFT result, good agreement of the calculated spectrum with the experimental C 1s core excitation spectrum of ANQ is achieved. The overestimation of the CVS-ADC(2)-s method is also practically constant with an absolute error of 3.7 to 3.9 eV. Considering the previously discussed results of the CVS-ADC(2)-x method, both CVS-ADC(2) methods are in case of ANQ more precise than TD-DFT/B3LYP with respect to absolute errors in excitation energies, as well as energy differences between the states.

With mean errors of about 0.32 eV (0.02%) and 5.1 eV (−0.2%), respectively, the C 1s and S 1s excited states of BT are also well described with CVS-ADC(2)-x. Here, TD-DFT provides an accurate energy spacing between the bright states with small standard deviation of only 0.03%, while the one of CVS-ADC(2)-x is slightly larger with 0.16%. The thymine data with mean errors of 0.11%, 0.02,% and −0.15% for the C, N, and O 1s core-excited states, respectively, show again the best results for CVS-ADC(2)-x.

The calculated results of the PTCDA C 1s excitations with the small 6–31G** basis set exhibit also the best agreement with the experimental values at the CVS-ADC(2)-x level. The energy gap between the two bright experimental peaks is 1.2 eV, while TD-DFT/B3LYP provides 1.57 eV, CVS-ADC(2)-s 1.51 eV, and CVS-ADC(2)-x 1.48 eV. Turning to the porphin N 1s excitations, the energy difference between the second and third experimental peak has been strongly underestimated using CVS-ADC(2)-x/6–31++G**. However, also TD-DFT/B3LYP and CVS-ADC(2)-s provide energy differences of similar magnitude. These findings are a further hint, that the calculations in

Table 10. Comparison of excitation energies (ω_{ex}) and oscillator strengths (f_{osc}) of the first eight O 1s singlet and triplet excited states of ANQ calculated with CVS-ADC(2)-s/x and TD-DFT/B3LYP with experimental values.[78]

	B3LYP		CVS-ADC(2)-s		CVS-ADC(2)-x		Expt.
State	ω_{ex}[eV]	f_{osc}	ω_{ex}[eV]	f_{osc}	ω_{ex}[eV]	f_{osc}	ω_{ex}[eV]
1	514.97 (T)	–	531.58 (T)	–	528.99 (T)	–	
2	514.97 (T)	–	531.58 (T)	–	528.99 (T)	–	
3	515.69 (S)	0.0284	532.17 (S)	0.0002	529.45 (S)	0.0002	
4	515.70 (S)	0.0338	532.17 (S)	0.0640	529.45 (S)	0.0689	529.2–531.4
5	517.33 (T)	–	534.21 (T)	–	533.08 (S)	–	
6	517.34 (S)	0.0005	534.21 (T)	–	533.08 (S)	0.0003	
7	517.34 (T)	–	534.21 (S)	0.0001	533.09 (T)	–	
8	517.35 (S)	0.0005	534.21 (S)	0.0006	533.09 (T)	–	

The calculations have been performed using the 6–311++G** basis set.

Table 11. Comparison of excitation energies (ω_{ex}) and oscillator strengths (f_{osc}) of the first spectroscopic bright C 1s singlet excited states of ANQ calculated using CVS-ADC(2)-s/x and TD-DFT/B3LYP with experimental values.[2]

	B3LYP		CVS-ADC(2)-s		CVS-ADC(2)-x		Expt.
Bright state	ω_{ex}[eV]	f_{osc}	ω_{ex}[eV]	f_{osc}	ω_{ex}[eV]	f_{osc}	ω_{ex}[eV]
1	273.28	0.015	287.76	0.051	284.40	0.038	284.1
2	273.53	0.040	288.10	0.155	284.78	0.041	
3	273.63	0.058			284.81	0.086	284.45
4	273.75	0.007	288.33	0.029	284.96	0.036	
5	273.77	0.026	288.36	0.060			284.8
6	274.02	0.023	288.63	0.011	285.27	0.024	
7			288.71	0.030			285
8					285.60	0.014	
9	274.59	0.060	289.10	0.029	285.74	0.028	
10	274.96	0.016	289.30	0.015	285.92	0.034	285.6
11	274.97	0.045	289.45	0.112	285.92	0.089	
12	275.06	0.023			286.13	0.014	
13					286.34	0.007	

The calculations have been performed using the 6–311++G** basis set and exploiting C_{2v} point group symmetry.

vacuum might not be adequate for the description of the third peak of the experimental solid-state spectrum. However, CVS-ADC(2)-x provides the best overall agreement with respect to the excitation energies and energy differences between the N 1s core-excited states of porphin.

Table 12 provides the arithmetic mean errors of the excitation energies with respect to experimental data for each type of core excitation averaged over all molecules investigated in this work. Going from the carbon atom to the heavier oxygen, the mean error at the TD-DFT level changes from −10.97 to −14.62 eV, while the relative error is reduced by approximately 1.1%. A similar trend is observed at the CVS-ADC(2)-x level, where the error changes from 0.25 to −0.73 eV. However, the errors are about 50 times smaller than the TD-DFT ones and they are close to zero. While core excitation energies from the carbon 1s levels are on average slightly overestimated, the results for oxygen and nitrogen are slightly underestimated. With values between −0.14% and 0.09%, the range of relative errors is much smaller compared to TD-DFT. CVS-ADC(2)-s provides an opposite trend with the largest mean error of 3.58 eV for C 1s core-excitations and only 1.81 eV for the O 1s ones. Therefore, the relative error decreases from 1.24% to 0.34% going from carbon to oxygen. However, the absolute values are larger compared to the extended variant CVS-ADC(2)-x. The reason for the variations for different kinds of atoms is due to the larger relativistic effects for heavier atoms that are not included neither in the CVS-ADC calculations nor in the TD-DFT ones. More accurate results are obtained using the extended version of CVS-ADC(2), because the double excitations are treated in first order of perturbation theory, while the strict version includes only the zeroth order terms. This leads to a better description of orbital relaxation effects in the core-excited states, thereby reducing the errors in the results. The pronounced underestimation of excitation energies of core-excited states by TD-DFT is most likely due to unbalanced SIE in core and valence orbitals resulting in a much too small energy gap between core and valence orbitals.

In summary, the following general conclusion can be drawn from the investigated molecules in this article. CVS-ADC(2)-x in combination with the 6–311++G** basis set reproduces the experimental results most accurately for the molecules investigated in this work, because it offers a fortuitous compensation of errors due to basis set, orbital relaxation, electron correlation, and neglect of relativistic effects. TD-DFT/B3LYP strongly underestimates the excitation energies of core-excited states compared to the experimental values up to 14.62 eV in case of oxygen 1s excitations. The absolute errors of the TD-DFT/B3LYP calculations are comparatively constant with 10–16 eV. Absolute shifts of the excitation energies are thus mandatory for calculations of core excitation spectra with TD-DFT/B3LYP. CVS-ADC(2)-s conversely, slightly overestimates the excitation energies of the core-excited states compared to the experimental values. However, with relative mean errors between 0.34% and 1.24%, the error is significantly smaller than in the

Table 12. Comparison of the calculated mean errors and the standard deviations σ of the excitation energies obtained with the 6–311++G** basis set with respect to experimental data for the different types of core excitations and different methods.

	B3LYP		CVS-ADC(2)-s		CVS-ADC(2)-x	
Core	Mean	σ	Mean	σ	Mean	σ
O 1s	−14.62 (−2.83)	0.27 (0.05)	1.81 (0.34)	0.32 (0.06)	−0.73 (−0.14)	0.17 (0.03)
N 1s	−13.19 (−3.39)	0.49 (0.14)	2.58 (0.64)	0.11 (0.02)	−0.27 (−0.07)	0.51 (0.13)
C 1s	−10.97 (−3.99)	0.29 (0.10)	3.58 (1.24)	0.28 (0.10)	0.25 (0.09)	0.25 (0.09)

The means are taken over all molecules and all core excitations of the respective type. The mean errors are given in eV. Additionally, relative errors in % are provided in parentheses.

case of TD-DFT/B3LYP. The standard deviations with about 0.1% are very similar for all three methods. Therefore, the core excitation spectra are in general well described with all tested methods. It should be noted that the statistics presented above are collected on the basis of only a few selected examples, thus they cannot be taken as general.

Conclusion

In this work, we have presented results of our implementation of strict and extended CVS-ADC(2) for the calculation of X-ray absorption spectra. Applying the CVS to the ADC working equations leads to a reduction of the ADC equations, as the interaction between core and valence-excited states is weak as the energy difference between core and valence orbitals is large. As a consequence, the corresponding Coulomb integrals are very small and can thus be neglected. The restriction of the index space of the ADC matrix elements to core excitations and the neglect of Coulomb integrals make CVS-ADC(2) a computationally very efficient method, with which core-excited electronic states are obtained directly. Our implementation features excitation energies of singlet, as well as triplet electronic states and properties like oscillator strengths. Furthermore, the procedure is parallelized and features the use of point group symmetry.

To test our implementation, we have chosen molecules of current interest in the areas of organic electronics (ANQ, BT, PTCDA) and biology (porphin, thymine). The core-excited states have been calculated using our implementation of CVS-ADC(2)-s and -x as well as TD-DFT/B3LYP. The results have been compared with experimental data from the literature. It could be shown that the best results are provided by the CVS-ADC(2)-x method in combination with the 6-311++G** basis set. The deviation of the absolute excitation energies to the experiment is in most of the cases around 0.1%–0.2%. It should be noted that the ADC method like any other post-HF method is sensitive to the chosen basis set, and therefore, the usage of a smaller basis set leads to a stronger overestimation and accordingly to larger differences to the experimental values. The high accuracy provided by CVS-ADC(2)-x can be explained by means of the stronger inclusion of doubly excited configurations. As core-excited states are very high in energy with an energetically large core-hole separation, orbital relaxation effects are important. CVS-ADC(2) captures these effects indirectly by means of the double excitations. The strict CVS-ADC(2) version generally overestimates the excitation energies in our calculations up to 1.5% depending on the molecule and used basis set. Compared to the extended variant, the double amplitudes are treated in zeroth order of perturbation theory, while CVS-ADC(2)-x also includes the first-order terms and, therefore, shows better agreement with experimental values. Besides the excellent agreement of the computed and experimental excitation energies, the energy spacing between the states is also well described within the extended variant of CVS-ADC(2). Especially, for the C 1s spectrum of ANQ, the results are very precise. In addition to the treatment of orbital relaxation and in combination with the 6–311++G** basis set, CVS-ADC(2)-x offers fortuitous error compensation of basis set incompleteness, electron correlation, and neglect of relativistic effects that leads to an almost perfect agreement with experimental data.

In all our calculations, TD-DFT shows strong but almost constant underestimation of the core excitation energies ranging from 2% to 5%. The reason is the electron SIE inherent in the standard B3LYP functional. However, TD-DFT/B3LYP provides in some cases excellent results for the energy spacing between dipole allowed states, for example for the C 1s spectrum of BT, but there are other examples like the thymine C 1s spectrum, where TD-DFT/B3LYP produces large errors for the bright states, thereby clearly limiting its predictive power. Overall, one can obtain acceptable core-absorption spectra with TD-DFT/B3LYP by adding a large constant shift to the absolute energies in particular having the low computational cost of TD-DFT compared to ADC(2) in mind. However, an experimental spectrum is always mandatory for interpreting TD-DFT results quantitatively.

Eventually, we have demonstrated the excellent performance of CVS-ADC(2)-x for the calculation of XAS spectra of medium-sized molecules that can be used as benchmark method of TD-DFT xc functionals. Furthermore, the initial excitation process of an ICD process after a core excitation can be described by CVS-ADC(2)-x and used to calculate possible ICD channels in the future. Prospective work will also concentrate on open-shell ion and radical systems as well as an implementation of CVS-ADC(3) that may lead to even more precise results.

Acknowledgment

JW gratefully acknowledges the Heidelberg Graduate School of Mathematical and Computational Methods for the Science for their support.

Keywords: x-ray absorption spectroscopy · NEXAFS · CVS-ADC(2) · organic electronics · core-excited states · electronic structure theory · thymine · porphin · acenaphthenequinone · bithiophene · PTCDA

How to cite this article: J. Wenzel, M. Wormit, A. Dreuw. *J. Comput. Chem.* **2014**, *35*, 1900–1915. DOI: 10.1002/jcc.23703

Additional Supporting Information may be found in the online version of this article.

[1] S. G. Urquhart, H. Ade, M. Rafailovich, J. S. Sokolov, Y. Zhang, *Chem. Phys. Lett.* **2000**, *322*, 412.
[2] F. Holch, D. Hübner, R. Fink, A. Schöll, E. Umbach, *J. Electron. Spectrosc. Relat. Phenom.* **2011**, *184*, 452.
[3] J. Stöhr, NEXAFS Spectroscopy; Springer: Berlin, **1992**.
[4] V. Feyer, O. Plekan, R. Richter, M. Coreno, M. de Simone, K. C. Prince, A. B. Trofimov, I. L. Zaytseva, J. Schirmer, *J. Phys. Chem. A* **2010**, *114*, 10270.
[5] Y. Zubavichus, A. Shaporenko, M. Grunze, M. Zharnikov, *J. Phys. Chem. A* **2005**, *109*, 6998.
[6] H. Ikeura-Sekiguchi, T. Sekiguchi, *Surf. Interface Anal.* **2008**, *40*, 673.
[7] S. G. Urquhart, H. Ade, *J. Phys. Chem. B* **2002**, *106*, 8531.
[8] G. Hähner, *Chem. Soc. Rev.* **2006**, *35*, 1244.
[9] C. Vahlberg, M. Linares, P. Norman, K. Uvdal, *J. Phys. Chem. C* **2012**, *116*, 796.
[10] L. S. Cederbaum, J. Zobeley, F. Tarantelli, *Phys. Rev. Lett.* **1997**, *79*, 4778.
[11] S. Marburger, O. Kugeler, U. Hergenhahn, T. Möller, *Phys. Rev. Lett.* **2003**, *90*, 203401.

[12] T. Jahnke, H. Sann, T. Havermeier, K. Kreidi, C. Stuck, M. Meckel, M. Schöffler, N. Neumann, R. Wallauer, S. Voss, A. Czasch, O. Jagutzki, A. Malakzadeh, F. Afaneh, T. Weber, H. Schmidt-Böcking, R. Dörner, *Nat. Phys.* **2010**, *6*, 139.
[13] U. Hergenhahn, *J. Electron. Spectrosc. Relat. Phenom.* **2011**, *184*, 78.
[14] K. Gokhberg, P. Kolorenč, A. I. Kuleff, L. S. Cederbaum, *Nature* **2014**, *505*, 661.
[15] F. Trinter, M. S. Schöffler, H. K. Kim, F. P. Sturm, K. Cole, N. Neumann, A. Vredenborg, J. Williams, I. Bocharova, R. Guillemin, M. Simon, A. Belkacem, A. L. Landers, T. Weber, H. Schmidt-Böcking, R. Dörner, T. Jahnke, *Nature* **2014**, *505*, 664.
[16] E. Runge, E. K. U. Gross, *Phys. Rev. Lett.* **1984**, *52*, 997.
[17] E. K. U. Gross, W. Kohn, *Phys. Rev. Lett.* **1985**, *55*, 2850.
[18] E. K. U. Gross, W. Kohn, *Adv. Quantum Chem.*, **1990**, *21*, 255.
[19] A. Dreuw, M. Head-Gordon, *Chem. Rev.* **2005**, *105*, 4009.
[20] F. A. Asmuruf, N. A. Besley, *Chem. Phys. Lett.* **2008**, *463*, 267.
[21] N. A. Besley, F. A. Asmuruf, *Phys. Chem. Chem. Phys.* **2010**, *12*, 12024.
[22] L. Yang, H. Ågren, V. Carravetta, L. G. M. Pettersson, *Phys. Scr.* **1996**, *54*, 614.
[23] J. Vinson, J. J. Rehr, J. J. Kas, E. L. Shirley, *Phys. Rev. B* **2011**, *83*, 115106.
[24] G. D. Purvis, III, R. J. Bartlett, *J. Chem. Phys.* **1982**, *76*, 1910.
[25] S. Coriani, T. Fransson, O. Christiansen, P. Norman, *J. Chem. Theory Comput.* **2012**, *8*, 1616.
[26] S. Coriani, O. Christiansen, T. Fransson, P. Norman, *Phys. Rev. A*, **2012**, *85*, 022507.
[27] O. Christiansen, H. Koch, P. Jørgensen, *Chem. Phys. Lett.* **1995**, *243*, 409.
[28] T. Fransson, S. Coriani, O. Christiansen, P. Norman, *J. Chem. Phys.* **2013**, *138*, 124311.
[29] M. Alagia, E. Bodo, P. Decleva, S. Falcinelli, A. Ponzi, R. Richter, S. Stranges, *Phys. Chem. Chem. Phys.* **2013**, *15*, 1310.
[30] M. Wormit, D. R. Rehn, P. H. P. Harbach, J. Wenzel, C. M. Krauter, E. Epifanovsky, A. Dreuw, *Mol. Phys.* **2014**, *112*, 774.
[31] J. Schirmer, *Phys. Rev. A* **1982**, *26*, 2395.
[32] J. Schirmer, A. B. Trofimov, *J. Chem. Phys.* **2004**, *120*, 11449.
[33] J. H. Starcke, M. Wormit, J. Schirmer, A. Dreuw, *Chem. Phys.* **2006**, *329*, 39.
[34] J. H. Starcke, M. Wormit, A. Dreuw, *J. Chem. Phys.* **2009**, *131*, 144311.
[35] P. H. P. Harbach, M. Wormit, A. Dreuw, *J. Chem. Phys.*, **2014**, accepted for publication.
[36] P. H. P. Harbach, A. Dreuw, In Modeling of Molecular Properties; P. Comba, Ed.; Wiley-VCH Verlag: Weinheim, Germany, **2011**.
[37] L. S. Cederbaum, W. Domcke, J. Schirmer, *Phys. Rev. A* **1980**, *22*, 206.
[38] A. Barth, L. S. Cederbaum, *Phys. Rev. A* **1981**, *23*, 1038.
[39] A. Barth, J. Schirmer, *J. Phys. B At. Mol. Phys.* **1985**, *18*, 867.
[40] O. Plekan, V. Feyer, R. Richter, M. Coreno, M. de Simone, K. C. Prince, A. B. Trofimov, E. V. Gromov, I. L. Zaytseva, J. Schirmer, *Chem. Phys.* **2008**, *347*, 360.
[41] A. B. Trofimov, T. E. Moskovskaya, E. V. Gromov, H. Köppel, J. Schirmer, *Phys. Rev. A* **2001**, *64*, 022504.
[42] A. B. Trofimov, T. E. Moskovskaya, E. V. Gromov, N. M. Vitkovskaya, J. Schirmer, *J. Struct. Chem.* **2000**, *41*, 483.
[43] C. Møller, M. S. Plesset, *Phys. Rev.* **1934**, *46*, 618.
[44] E. R. Davidson, *J. Comp. Phys.* **1975**, *17*, 87.
[45] Y. Shao, L. F. Molnar, Y. Jung, J. Kussmann, C. Ochsenfeld, S. T. Brown, A. T. B. Gilbert, L. V. Slipchenko, S. V. Levchenko, D. P. O'Neill, R. A. J. DiStasio, R. C. Lochan, T. Wang, G. J. O. Beran, N. A. Besley, J. M. Herbert, C. Y. Lin, T. Van Voorhis, S. H. Chien, A. Sodt, R. P. Steele, V. A. Rassolov, P. E. Maslen, P. P. Korambath, R. D. Adamson, B. Austin, J. Baker, E. F. C. Byrd, H. Dachsel, R. J. Doerksen, A. Dreuw, B. D. Dunietz, A. D. Dutoi, T. R. Furlani, S. R. Gwaltney, A. Heyden, S. Hirata, C.-P. Hsu, G. Kedziora, R. Z. Khalliulin, P. Klunzinger, A. M. Lee, M. S. Lee, W. Liang, I. Lotan, N. Nair, B. Peters, E. I. Proynov, P. A. Pieniazek, Y. M. Rhee, J. Ritchie, E. Rosta, C. D. Sherrill, A. C. Simmonett, J. E. Subotnik, H. L. I. Woodcock, W. Zhang, A. T. Bell, A. K. Chakraborty, D. M. Chipman, F. J. Keil, A. Warshel, W. J. Hehre, H. F. I. Schaefer, J. Kong, A. I. Krylov, P. M. W. Gill, M. Head-Gordon, *Phys. Chem. Chem. Phys.* **2006**, *8*, 3172.
[46] E. Epifanovsky, M. Wormit, T. Kuś, A. Landau, D. Zuev, K. Khistyaev, P. Manohar, I. Kaliman, A. Dreuw, A. I. Krylov, *J. Comput. Chem.* **2013**, *34*, 2293.
[47] G. Fronzoni, R. De Francesco, M. Stener, P. Decleva, *J. Chem. Phys.* **2007**, *126*, 134308.
[48] F. Weigend, R. Ahlrichs, *Phys. Chem. Chem. Phys.***2005**, *7*, 3297.
[49] F. Weigend, M. Häser, *Theor. Chem. Acc.* **1997**, *97*, 331.
[50] C. Hättig, F. Weigend, *J. Chem. Phys.* **2000**, *113*, 5154.
[51] F. Weigend, M. Häser, H. Patzelt, R. Ahlrichs, *Chem. Phys. Lett.* **1998**, *294*, 143.
[52] F. Weigend, *Phys. Chem. Chem. Phys.* **2006**, *8*, 1057.
[53] S. Kossmann, F. Neese, *J. Chem. Theory Comput.* **2010**, *6*, 2325.
[54] C. Lee, W. Yang, R. G. Parr, *Phys. Rev. B* **1988**, *37*, 785.
[55] A. D. Becke, *J. Chem. Phys.* **1993**, *98*, 5648.
[56] A. D. Becke, *J. Chem. Phys.* **1993**, *98*, 1372.
[57] R. Ahlrichs, M. Bär, M. Häser, H. Horn, C. Kölmel, *Chem. Phys. Lett.* **1989**, *162*, 165.
[58] F. Neese, *Wiley Interdiscip. Rev. Comput. Mol. Sci.* **2012**, *2*, 73.
[59] M. Stener, G. Fronzoni, M. de Simone, *Chem. Phys. Lett.* **2003**, *373*, 115.
[60] S. DeBeer George, T. Petrenko, F. Neese, *J. Phys. Chem. A* **2008**, *112*, 12936.
[61] R. Krishnan, J. S. Binkley, R. Seeger, J. A. Pople, *J. Chem. Phys.* **1980**, *72*, 650.
[62] A. D. McLean, G. S. Chandler, *J. Chem. Phys.* **1980**, *72*, 5639.
[63] W. J. Hehre, R. Ditchfield, J. A. Pople, *J. Chem. Phys.* **1972**, *56*, 2257.
[64] P. C. Hariharan, J. A. Pople, *Theor. Chim. Acta* **1973**, *28*, 213.
[65] T. Clark, J. Chandrasekhar, G. W. Spitznagel, P. V. R. Schleyer, *J. Comput. Chem.* **1983**, *4*, 294.
[66] I. Bâldea, B. Schimmelpfennig, M. Plaschke, J. Rothe, J. Schirmer, A. B. Trofimov, T. Fanghänel, *J. Electron. Spectrosc. Relat. Phenom.* **2007**, *154*, 109.
[67] V. Feyer, O. Plekan, R. Richter, M. Coreno, G. Vall-llosera, K. C. Prince, A. B. Trofimov, I. L. Zaytseva, T. E. Moskovskaya, E. V. Gromov, J. Schirmer, *J. Phys. Chem. A* **2009**, *113*, 5736.
[68] N. S. Lewis, *Science* **2007**, *315*, 798.
[69] A. L. Roes, E. A. Alsema, K. Blok, M. K. Patel, *Prog. Photovolt: Res. Appl.* **2009**, *17*, 372.
[70] M. Katsuhara, I. Yagi, A. Yumoto, M. Noda, N. Hirai, R. Yasuda, T. Moriwaki, S. Ushikura, A. Imaoka, T. Urabe, K. Nomoto, *J. Soc. Inf. Disp.* **2010**, *18*, 399.
[71] S.-Y. Chang, H.-C. Liao, Y.-T. Shao, Y.-M. Sung, S.-H. Hsu, C.-C. Ho, W.-F. Su, Y.-F. Chen, *J. Mater. Chem. A* **2013**, *1*, 2447.
[72] J. Wenzel, A. Dreuw, I. Burghardt, *Phys. Chem. Chem. Phys.* **2013**, *15*, 11704.
[73] J. Cremer, E. Mena-Osteritz, N. G. Pschierer, K. Müllen, P. Bäuerle, *Org. Biomol. Chem.* **2005**, *3*, 985.
[74] A. Petrella, J. Cremer, L. De Cola, P. Bäuerle, R. M. Williams, *J. Phys. Chem. A* **2005**, *109*, 11687.
[75] L. X. Chen, S. Xiao, L. Yu, *J. Phys. Chem. B* **2006**, *110*, 11730.
[76] L. Huo, J. Hou, S. Zhang, H. Y. Chen, Y. Yang, *Angew. Chem. Int. Ed.* **2010**, *49*, 1500.
[77] T. Roland, J. Léonard, G. H. Ramirez, S. Méry, O. Yurchenko, S. Ludwigs, S. Haacke, *Phys. Chem. Chem. Phys.* **2012**, *14*, 273.
[78] N. Schmidt, T. Clark, S. G. Urquhart, R. H. Fink, *J. Chem. Phys.* **2011**, *135*, 144301.
[79] T. Roland, G. H. Ramirez, J. Léonard, S. Méry, S. Haacke, *J. Phys. Conf. Ser.* **2011**, *276*, 012006.
[80] J. L. Brédas, G. B. Street, B. Thémans, J. M. André, *J. Chem. Phys.* **1985**, *83*, 1323.
[81] C. Quattrocchi, R. Lazzaroni, J. L. Brédas, *Chem. Phys. Lett.* **1993**, *208*, 120.
[82] A. Karpfen, C. H. Choi, M. Kertesz, *J. Phys. Chem. A* **1997**, *101*, 7426.
[83] P. M. Viruela, R. Viruela, E. Orti, *Int. J. Quantum Chem.* **1998**, *70*, 303.
[84] P. Väterlein, M. Schmelzer, J. Taborski, T. Krause, F. Viczian, M. Bäßler, R. Fink, E. Umbach, W. Wurth, *Surf. Sci.* **2000**, *452*, 20.
[85] S. Narioka, H. Ishii, Y. Ouchi, T. Yokoyama, T. Ohta, K. Seki, *J. Phys. Chem.* **1995**, *99*, 1332.
[86] G. Polzonetti, V. Carravetta, G. Iucci, A. Ferri, G. Paolucci, A. Goldoni, P. Parent, C. Laffon, M. V. Russo, *Chem. Phys.* **2004**, *296*, 87.
[87] A. Nakata, Y. Imamura, T. Otsuka, H. Nakai, *J. Chem. Phys.* **2006**, *124*, 094105.
[88] C. Vahlberg, M. Linares, S. Villaume, P. Norman, K. Uvdal, *J. Phys. Chem. C* **2011**, *115*, 165.
[89] A. J. Atkins, C. R. Jacob, M. Bauer, *Chem. Eur. J.* **2012**, *18*, 7021.

Received: 5 June 2014
Revised: 18 July 2014
Accepted: 21 July 2014
Published online on 7 August 2014